Semicond. Sci. Technol. **14** (1999) 532–542. Printed in the UK PII: S0268-1242(99)99473-7

Towards the Monte Carlo simulation of resonant tunnelling diodes using time-dependent wavepackets and Bohm trajectories

X Oriols†, J J García-García†, F Martín†, J Suñé†‖, J Mateos‡, T González‡, D Pardo‡ and O Vanbésien§

† Departament d'Enginyeria Electrònica, Universitat Autonoma de Barcelona, 08193 Bellaterra, Spain
‡ Departamento de Física Aplicada, Universidad de Salamanca, 37008 Salamanca, Spain
§ Institute d'Electronique et Microélectronique du Nord UMR CNRS 9929, Université des Sciences et Technologies de Lille, Avenue Poincare BP69, 59652 Villeneuve D'Ascq Cedex, France

E-mail: xoriols@cc.uab.es

Received 16 November 1998, accepted for publication 11 March 1999

Abstract. Following the path of a previous letter, a generalization of the classical Monte Carlo (MC) device simulation technique is proposed with the final goal of simultaneously dealing with phase-coherence effects and scattering interactions in quantum-based devices. The proposed method is based on time-dependent wavepackets and Bohm trajectories and restricts the quantum treatment of transport to the device regions where the potential profile significantly changes in distances of the order of the de Broglie wavelength of the carriers (the quantum window). Outside this region, electron transport is described in terms of the semiclassical Boltzmann equation, which is solved using the MC technique. In this paper, our proposed description for the electron ensemble inside the quantum window is rewritten in terms of the density matrix. It is shown that, neglecting scattering, the off-diagonal terms of the density matrix remain identically zero even if time-dependent wavepackets are used. Bohm trajectories in tunnelling scenarios are reviewed to show their feasibility to extend the MC technique to mesoscopic devices. A self-consistent one-dimensional simulator for resonant tunnelling diodes has been developed to technically validate our proposal. The obtained simulation results are promising and encourage further efforts to include quantum effects into MC simulations.

1. Introduction

Extrapolations of the actual tendency of miniaturization of integrated circuits (ICs) predict that the minimum dimensions of conventional semiconductor devices will enter into the sub 100 nm range by the beginning of the next century [1]. The wave character of the charge carriers will certainly influence any further scaling of conventional transistors, and novel devices based on quantum mechanical (QM) and/or single-electron effects are expected to open a new path toward faster, lower-consumption and more compact semiconductor ICs. Among other QM phenomena, tunnelling is one of the effects which are presumed to play an important role in future ICs. The well-known resonant tunnelling diode (RTD) is expected to play a relevant role in the improvement of both analogue (microwave source [2]) and digital (high-speed electronics [3]) circuits.

Although RTDs have been thoroughly studied during the past 25 years, it is only recently that a quantitative comparison with experiment has given reasonable results [4, 5]. In addition to the inherent limitations for reaching agreement between theory and experiment whenever tunnelling is involved (it depends exponentially on many parameters such as barrier height and thickness), the main difficulties for the accurate modelling of these devices are related to (i) reasonable 'open system' boundary conditions [6, 7] and (ii) the simultaneous consideration of phase-coherence effects and of scattering interactions. Different approaches have been taken to face these difficult problems. Full quantum-kinetic treatments of electron transport, based on obtaining the Wigner distribution function [8–12] or using a Green function approach [4, 5, 13, 14], are generally considered to be necessary. However, although a recent reformulation of the nonequilibrium Green function theory by Lake *et al* [4] has given very good results, they have extremely high computational requirements. In this regard,

‖ To whom all correspondence should be addressed.

0268-1242/99/060532+11$19.50

efforts devoted to more phenomenological approaches can also enlighten our understanding of quantum-based devices. Several publications follow this direction [15–19]. Among them, the work of Fischetti [17], which suggests the use of the Pauli master equation, is particularly interesting because it starts a discussion about the actual need for fully off-diagonal formulations of quantum transport to deal with the devices of interest. On the other hand, Rossi *et al* [18] have developed a density matrix formulation to include scattering inside the dynamics of a single time-dependent wavepacket. In the present work, we follow the path initiated by Salvino and Buot [16] who proposed a semiclassical Monte Carlo (MC) simulator for RTDs considering quantum trajectories in the double-barrier region. In this regard our main goal is to present a proposal to deal with electron transport in quantum devices which is simultaneously reliable and intuitive. In a previous letter [20], we have shown the technical viability of a quantum MC simulator based on Bohm trajectories associated with time-dependent wavepackets. In the present paper, particular interest is devoted to giving an alternative view of our model for electron transport in terms of the density matrix, to briefly review the phenomenology of tunnelling with Bohm trajectories and to discuss several possibilities to include scattering.

The paper is organized as follows. In section 2, an introduction to our model is presented and it is reformulated in terms of the density matrix. Section 3 is devoted to analysing the properties of Bohm trajectories in tunnelling devices, with emphasis on double-barrier structures. The general features of the quantum MC simulator for RTDs are discussed in section 4. Several considerations about scattering are presented. Finally, section 5 presents the results obtained with this new technique and points out directions for future work.

2. Time-dependent wavepackets

As previously indicated, the main goal of the present work is to explore the possibilities of extending the semiclassical MC technique to mesoscopic devices by means of wavepackets and Bohm trajectories. However, in order to consider large integration boxes without unnecessary computational burden, quantum-transport models are restricted to a small portion of the device that we call the quantum window (QW). Actually, we deal with vertical transport devices which can be modelled using a one-dimensional picture and we distinguish three regions in the device: the emitter region, the QW and the collector region.

The emitter and collector regions, close to the respective contacts, are treated as semiclassical regions. From an ensemble MC simulation of particles at these semiclassical regions one can deduce a semiclassical distribution function at the limits of the QW. Each electron that enters into the QW is associated with an initial Gaussian wavepacket whose energy is directly related to its classical counterpart. The dynamics of this electron inside the QW is directly related to the wavepacket evolution.

Let us note that the electron dynamics is determined by ordinary classical forces at the semiclassical regions. However, these classical forces are rigorously deduced by considering the QM evolution of a wavepacket when the externally applied electric field varies slowly over the dimensions of such a wavepacket [21]. This semiclassical model recovers the classical picture of an electron as a particle and forgets its original wavepacket description. However, within actual devices whose dimensions can be comparable with the electron de Broglie wavelength, the quantum nature of electrons can no longer be neglected. In this regard, the electron description inside the QW by wavepackets seems the most natural extension of the classical MC technique to quantum devices.

In previous work [20], we have explained our proposal for a quantum MC simulation based on the time-dependent Schrödinger equation (TDSE) in the effective mass framework. Now, a description in terms of the density matrix formalism will be presented, which provides a new point of view of our proposal which is closer to those most commonly used for the description of mesoscopic devices.

2.1. Density operator representation for the wavepacket dynamics inside the QW

As we have already mentioned, we associate an initial Gaussian wavepacket with each electron that enters into the QW. In particular, we consider minimum-uncertainty Gaussian wavepackets:

$$\psi_{k_c,t_0}(x,t_0)=\frac{1}{(\pi\sigma_x^2)^{1/4}}\exp\left[-\frac{(x-x_c)^2}{2\sigma_x^2}+\mathrm{i}k_c x\right] \tag{1}$$

σ_x being the spatial dispersion, x_c the spatial centre of the wavepacket at the initial time $t=t_0$ and k_c the central wavevector which is related to a central energy E_c. It is important to note that σ_x and x_c are identical for all electrons, but t_0 and k_c depend on each particular electron history. In order to avoid a time discretization of the TDSE which would not be convenient for a MC simulation, we have chosen to calculate $\psi_{k_c,t_0}(x,t)$ by superposition. Hence, we begin by integrating the stationary Schrödinger equation to obtain a basis of scattering eigenstates, $\{\Psi_k(x)\}$, and then we proceed to numerically project the initial wavepacket onto this basis:

$$\psi_{k_c,t_0}(x,t_0)=\int_{-\infty}^{\infty}a_{k_c}(k)\psi_k(x)\,\mathrm{d}k \tag{2}$$

with

$$a_{k_c}(k)=\int_{-\infty}^{\infty}\psi_k^*(x)\psi_{k_c,t_0}(x,t_0)\,\mathrm{d}x. \tag{3}$$

The Hamiltonian eigenfunctions $\Psi_k(x)$ are calculated following the procedure described in [22]. The main advantage of this method is that $\psi_{k_c,t_0}(x,t)$ can be computed by superposition at any arbitrary instant of time t:

$$\begin{aligned}\langle x|\psi_{k_c,t_0}(t)\rangle&=\psi_{k_c,t_0}(x,t)\\&=\int_{-\infty}^{\infty}a_{k_c}(k)\exp\left[-\mathrm{i}\frac{E(k)(t-t_0)}{\hbar}\right]\psi_k(x)\,\mathrm{d}k\end{aligned} \tag{4}$$

without having to calculate it at intermediate times. $E(k)$ is the energy associated with the scattering eigenstate $\Psi_k(x)$, related to the wavevector k via a parabolic dispersion relationship.

Moreover, since a single-particle system can be equivalently described by the Schrödinger or Liouville equation, the density operator for this single-electron system can be written as

$$\rho(t) = |\psi_{k_c,t_0}(t)\rangle\langle\psi_{k_c,t_0}(t)| \tag{5}$$

and the density matrix, represented in the Hamiltonian eigenstate basis $\{\Psi_k(x)\}$, can be easily expressed as

$$\rho_{k'k}(t) = \langle\psi_{k'}|\psi_{k_c,t_0}(t)\rangle\langle\psi_{k_c,t_0}(t)|\psi_k\rangle$$
$$= a_{k_c}(k')a^*_{k_c}(k)\exp\left\{\mathrm{i}\frac{[E(k)-E(k')](t-t_0)}{\hbar}\right\}. \tag{6}$$

However, as we have pointed out, our quantum system is not composed of a single wavepacket but of an ensemble of them. In particular, it contains a constant flux of wavepackets that corresponds to a constant flux of electrons entering inside the QW at different initial times and with different energies. This picture can be summarized as follows: (i) each particle enters into the QW at a different initial time, t_0, and (ii) there is a distribution of the central wavevector $f(k_c, t_0)$ which can be obtained from the number of classical particles that arrive at the QW, from the emitter, at different times. The model can be easily generalized to also consider injection from the collector side to the QW. However, for simplicity, all the development will be done assuming only electrons incidents from the emitter. Since we are dealing with a pure coherent system (scattering is neglected in this preliminary version), $f(k_c, t_0)$ is position independent.

The density matrix representing the whole electron ensemble can be written taking into account the above two points. The first one implies a sum over all possible entering times, t_0, and the second point a statistical average in accordance with $f(k_c, t_0)$. If we suppose that the initial entering time is uniformly distributed from $-\infty$ to $+\infty$, the density operator can be written as:

$$\rho(t) = \int_0^\infty \mathrm{d}k_c\, f(k_c, t_0)\int_{-\infty}^{+\infty}|\psi_{k_c,t_0}(t)\rangle\langle\psi_{k_c,t_0}(t)|\,\mathrm{d}t_0. \tag{7}$$

Let us suppose that we are in a steady-state situation where $f(k_c, t_0)$ is time independent; then expression (7) can be largely simplified. If we use the identity

$$\frac{1}{2\pi}\int_{-\infty}^{\infty}\exp\left\{\mathrm{i}\frac{[E(k)-E(k')]t_0}{\hbar}\right\}\mathrm{d}t_0 = \frac{m^*}{\hbar}\frac{1}{k}\delta(k'-k) \tag{8}$$

then we find that each element of the density matrix can be rewritten as

$$\rho_{k'k}(t) = \int_0^\infty f(k_c)a_{k_c}(k')a^*_{k_c}(k)\exp\left\{\mathrm{i}\frac{[E(k)-E(k')]t}{\hbar}\right\}$$
$$\times 2\pi\frac{m^*}{\hbar}\frac{1}{k}\delta(k'-k)\,\mathrm{d}k_c. \tag{9}$$

At this point, let us note that, even working with time-dependent wavepackets (rather than with Hamiltonian eigenstates), we have found a diagonal density matrix for our coherent system under steady-state conditions. In the next section, we will use this property to compute the probability presence and the current density.

2.2. Time-dependent wavepackets versus Hamiltonian eigenstates

Once an expression for the density matrix is obtained (equation (9)), all observables can be determined. In this regard, we will compare the results for the probability presence and current densities obtained with our time-dependent wavepacket model and with a description based on the Hamiltonian eigenstates.

The probability presence density operator neglecting the spin in one-dimensional scenarios for the position and for the momentum variables can be represented in the $\{\Psi_k(x)\}$ basis by:

$$q_{kk'} = \psi^*_k(x)\psi_{k'}(x). \tag{10}$$

Hence, its related observable, $Q(x, t)$, is computed as

$$Q(x,t) = \int_{-\infty}^{\infty}\int_{-\infty}^{\infty} q_{kk'}\rho_{k'k}(t)\,\mathrm{d}k\,\mathrm{d}k'. \tag{11}$$

After using the δ function of expression (9), one obtains

$$Q(x,t) = 2\pi\frac{m^*}{\hbar}\int_0^\infty\int_{-\infty}^{\infty} f(k_c)|\psi_k(x)|^2\frac{|a_{k_c}(k)|^2}{k}\,\mathrm{d}k_c\,\mathrm{d}k. \tag{12}$$

The charge computed at any position inside the QW is time independent (a steady-state situation is considered) and depends on the modulus of $a_{k_c}(k)$. In particular, if the electron is described by a wavepacket with $a_{k_c}(k) = \delta(k-k_c)$ (i.e. a scattering state), then the standard expression for the probability presence density in coherent models based on stationary states is recovered:

$$Q(x,t) = 2\pi\frac{m^*}{\hbar}\int_0^\infty f(k,t)\frac{|\Psi_k(x)|^2}{k}\,\mathrm{d}k. \tag{13}$$

Now, let us proceed identically for the current density. The current density operator, $J_{kk'}$, in the $\{\Psi_k(x)\}$ basis is represented by [23]

$$J_{kk'} = \frac{\hbar}{2m^*\mathrm{i}}\left[\psi^*_k(x)\frac{\partial\psi_{k'}(x)}{\partial x} - \psi_{k'}(x)\frac{\partial\psi^*_k(x)}{\partial x}\right] \tag{14}$$

and then its related unidimensional observable $J(x, t)$ is

$$J(x,t) = 2\pi\frac{-\mathrm{i}}{2}\int_0^\infty\int_{-\infty}^{\infty} f(k_c)$$
$$\times\left[\psi^*_k(x)\frac{\partial\psi_k(x)}{\partial x} - \psi_k(x)\frac{\partial\psi^*_k(x)}{\partial x}\right]\frac{|a_{k_c}(k)|^2}{k}\,\mathrm{d}k_c\,\mathrm{d}k. \tag{15}$$

The current carried by a Hamiltonian eigenstate is position independent and related to its transmission coefficient, $T(k)$. Thus, we obtain

$$J(x,t) = \frac{\hbar}{m^*}\int_0^\infty\int_{-\infty}^{\infty} f(k_c)|a_{k_c}(k)|^2T(k)\,\mathrm{d}k_c\,\mathrm{d}k. \tag{16}$$

Hence, as defined for a steady-state situation, the current density is constant and uniform. Once again, by defining $a_{k_c}(k) = \delta(k-k_c)$, one recovers the standard expression for the current density in the scattering states picture:

$$J(x,t) = \frac{\hbar}{m^*}\int_{-\infty}^{\infty} f(k,t)T(k)\,\mathrm{d}k. \tag{17}$$

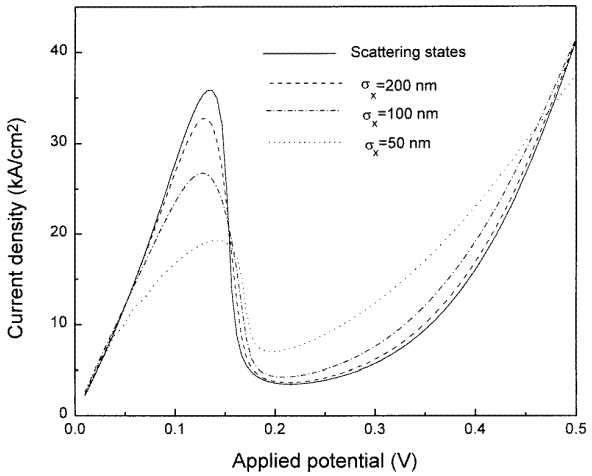

Figure 1. Non-self-consistent I–V curves for a typical RTD computed using scattering states or Gaussian wavepackets with different values of the spatial dispersion, σ_x.

Looking at expressions (16) and (17), the transmission coefficient for a time-dependent wavepacket can be easily identified [24]:

$$T(k_c) = \int_0^\infty |a_{k_c}(k)|^2 T(k)\,\mathrm{d}k. \tag{19}$$

As for the probability presence, the current density associated with a time-dependent wavepacket can be quite different from that associated with an eigenstate. In figure 1, we have represented the influence of the spatial dispersion, σ_x, on the I–V curve of a typical RTD (calculated non-self-consistently). In particular, we consider a symmetric double-barrier structure with 3 nm barriers of $Al_xGa_{1-x}As$, a 5 nm well of GaAs and highly doped ($N_D = 10^{18}$ cm^{-3}) GaAs electrodes. We remark that a significant peak-to-valley ratio is obtained for narrow wavepackets without the consideration of inelastic scattering. This dispersion in the results obtained from equations (12) and (16) (related to the arbitrary choice of σ_x) has been used to criticize our proposal. However, in the authors' opinion, this is an advantage rather than a drawback, since it introduces some flexibility regarding the modelling of the 'size of an electron', in the sense described by Fischetti [17]. In this way, regardless of technical or numerical difficulties, our proposal can *a priori* simulate classical particles by defining $\sigma_x \approx 0$ (i.e. $a_{k_c}(k) \approx cte$) and also scattering states $\sigma_x \approx \infty$ (i.e. $a_{k_c}(k) = \delta(k - k_c)$). Obviously, these two limiting situations lead to quite different macroscopic results, as we have seen in figure 1.

In conclusion, we have shown that, under steady-state conditions, the density matrix associated with the described quantum system is diagonal in the basis of the Hamiltonian eigenstates (equation (9)). This result has to be compared with the density matrix associated with a single time-dependent wavepacket (equation (6)), which is nondiagonal in the same representation. Moreover, the results obtained from expression (9) can be qualitatively different from the ones obtained with Hamiltonian eigenstates. Finally, let us note that expressions (12) and (16) can be equivalently deduced without appealing to the density matrix formalism, but this allows us to look at our picture from a different point of view and to compare it with other models. Moreover, and this is much more important, it reveals a possible path [18] for the introduction of scattering interactions within the QW.

3. Trajectories in Bohm's interpretation of quantum mechanics

Electron trajectories have been used to understand electron devices for decades. The successful use of these trajectories in classical MC simulators and the existence of trajectory formulations of the QM suggest the idea to extend their use to the simulation of quantum devices [16, 20]. Several advantages can be expected: (i) the matching between the classical and quantum regions (the electrons getting into and out of the QW) can be done in terms of individual trajectories, (ii) Bohm trajectories open the possibility to consider scattering as a local event and (iii) this would allow us to go on studying quantum devices without losing our intuitive picture for electronic transport.

As mentioned, several attempts have been made to describe the quantum dynamics in terms of causal trajectories of hidden variables. Among them, Bohm trajectories perfectly fit with our final goal since they have already been successfully applied to analyse the problem of tunnelling through potential barriers [25–27] and perfectly reproduce the charge and current densities.

3.1. Bohm's interpretation

Classically, a particle is dynamically described as a point in phase space which evolves according to Newton's second law or, equivalently, to the corresponding Hamilton–Jacobi equation. Standard QM in the Schrödinger picture substitutes this description by the use of a wavefunction $\Psi(x, t)$, which evolves according to the TDSE, and the notion of trajectory disappears. Bohm's formulation of QM mixes both types of descriptions, since it retains the concept of wavefunction and postulates the existence of well-defined causal particle trajectories. The evolution of a particle initially located at a position x_0 is uniquely determined by a Hamilton–Jacobi-like equation directly derived from the TDSE. A particle has (at each instant of time) a well-defined position and velocity causally determined by an objectively real (complex-valued) field directly related to $\Psi(x, t)$ (see Bohm's original paper for a detailed formulation [25]).

Consistently with Bohm's interpretation, once the wavefunction is completely determined by solving the TDSE, the velocity can be easily computed as

$$v(x, t) = \frac{1}{q}\frac{J(x, t)}{|\psi(x, t)|^2} \tag{20}$$

where q is the absolute value of the electron charge. Then, for any initial position x_0, the trajectory $x(x_0, t)$ is uniquely defined by integration. The relevant point is that, in Bohm's picture, a unique causal trajectory is found for each initial position x_0.

At this point we will discuss how the standard QM results can be exactly reproduced in terms of individual trajectories. Following Bohm's formulation, the initial

position is uncertain and only the presence probability density $|\Psi(x_0, 0)|^2$ is considered to be known at $t = 0$. According to this weak version of the Heisenberg uncertainty principle, the physical observables must be computed by averaging the corresponding magnitude $A(x_0, t)$ over all possible Bohm trajectories:

$$\langle A \rangle = \frac{\int_{-\infty}^{\infty} A(x_0, t)|\psi(x_0, 0)|^2 \, \mathrm{d}x_0}{\int_{-\infty}^{\infty} |\psi(x_0, 0)|^2 \, \mathrm{d}x_0}. \qquad (21)$$

The observables obtained from Bohm trajectories using equation (21) are identical to those calculated within the standard interpretation of QM. In particular, as a direct consequence of the continuity equation, the presence probability density at an arbitrary position x can be recovered by 'counting' all the particles, i.e.

$$|\psi(x, t)|^2 = \int_{-\infty}^{\infty} \mathrm{d}x_0 \, |\psi(x_0, 0)|^2 \delta[x - x(x_0, t)] \qquad (22)$$

and the current density by weighting their velocities:

$$J(x, t) = q \int_{-\infty}^{\infty} \mathrm{d}x_0 \, |\psi(x_0, 0)|^2 v(x, t) \delta[x - x(x_0, t)]. \qquad (23)$$

From the above two expressions, Bohm's approach can be considered as a mathematical tool which is able to reproduce the presence probability and current density associated with $\Psi(x, t)$ using well-defined particle trajectories. Moreover, since the main goal of any device simulator is to obtain charge densities (i.e. self-consistent potential profiles) and current fluxes, the two previous equations demonstrate that we can obtain reliable results using Bohm trajectories and treat the classical and quantum regions equivalently.

3.2. Phenomenology of Bohm trajectories in double-barrier structures

Since Bohm trajectories are absolutely determined by the Schrödinger equation, the initial wavefunction is the only degree of freedom available to model the particle's behaviour in different experimental situations. Two alternatives have been considered in the literature: time-independent eigenfunctions of the Hamiltonian (scattering states), and localized time-dependent wavepackets.

In particular, since the current density associated with scattering states is positive and position independent, Bohm's velocity is positive everywhere according to equation (20). This means that, although Bohm trajectories perfectly reproduce the presence probability and the current density of scattering states, they are all transmitted through the barrier. In this regard, these trajectories do not reproduce our particle-intuitive understanding of the tunnelling phenomenon and, as a consequence, their possible application to time-dependent electron transport simulation is hindered. However, we cannot conclude that Bohm's approach fails for scattering states, because it perfectly reproduces the results of standard QM also in this case. In other words, the apparent failure of Bohm's formulation applied to scattering states is due to undesired features of these time-independent states themselves in describing particle time-dependent phenomena [22].

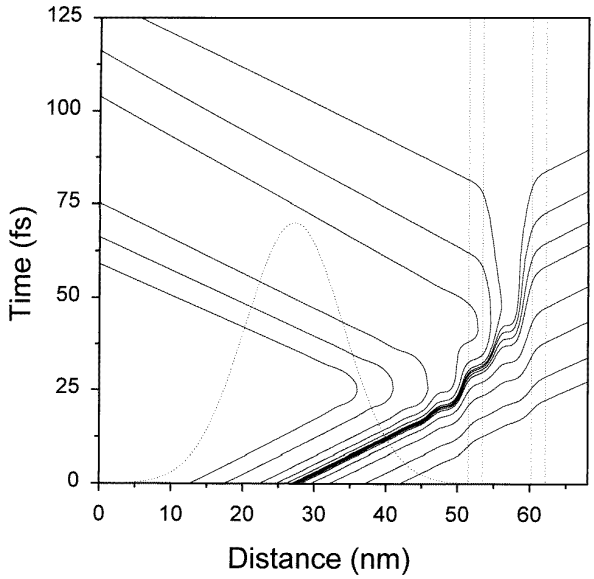

Figure 2. Bohm trajectories associated with an initial Gaussian wavepacket with a central energy of 0.22 eV and a spatial dispersion of 10 nm, impinging upon a double-barrier structure with 2 nm barriers of 0.3 eV and 7 nm well. The barriers and the initial Gaussian wavepacket are indicated by dotted lines.

The other alternative choice for the initial wavefunction is a time-dependent wavepacket (as that of equation (1)). Since these wavepackets are adequate to reproduce the electron dynamics, the associated Bohm trajectories will also provide a reliable description, even from the intuitive point of view. An example of trajectories associated to a time-dependent wavepacket will be shown.

Since we are interested in the simulation of RTDs, we have chosen the double-barrier structure to show the main features of Bohm trajectories in tunnelling structures. Let us study the tunnelling of electrons (described as Gaussian wavepackets of spatial dispersion $\sigma_x = 10$ nm) through a double-barrier structure with the following parameters: barrier height of 0.3 eV, barrier thickness of 2 nm, well width of 7 nm and uniform effective mass of $0.067m_0$ (Γ point of GaAs). In figure 2 we show the trajectories corresponding to the second transmission resonance ($E_c = 0.22$ eV) of the structure. The trajectories coming from the front of the wavepacket are transmitted, while those from the rear are reflected (most of them without even reaching the barrier). This is caused by the fact that Bohm trajectories do not cross each other in configuration space [28]. If the barrier region is limited by $x_L < x < x_R$, we can calculate the wavepacket transmission coefficient $T(k_c)$ by computing the probability presence at the right of point x_R for $t \to \infty$. Moreover, since we know that Bohm trajectories do not cross, T(k_c) can also be computed by counting all the transmitted particles:

$$T(k_c) = \int_{x_R}^{\infty} |\psi_{k_c}(x, t \to \infty)|^2 \, \mathrm{d}x$$
$$= \int_{-\infty}^{\infty} \alpha_T(x_0)|\psi_{k_c}(x_0, 0)|^2 \, \mathrm{d}x_0 \qquad (24)$$

where $\alpha_T(x_0)$ is equal to unity if the particle is transmitted and zero otherwise. Let us recall that it was not possible to reproduce the transmission and reflection coefficients of

stationary scattering states by counting transmitted Bohm trajectories (all stationary Bohm particles are transmitted). It is in this sense that we have argued that the stationary Bohm trajectories do not reproduce our intuitive picture of tunnelling.

We have already discussed how the measurable results of standard QM can be obtained by averaging the involved magnitude over all Bohm trajectories. However, Bohm's interpretation also provides other results which do not have a counterpart within the standard framework. This is not surprising since the causal trajectories give a deeper structure to the quantum theory. Within Bohm's interpretation, concepts such as the momentum of particles at a given position, the arrival time or the transit time between two points are defined for individual particles in a natural way. The distribution of these magnitudes can also be obtained by taking into account all the trajectories with their corresponding probabilities. All these results do not have an analogue within the standard interpretation of QM and should be regarded with caution until Bohm's hidden theory is confirmed or refuted by experiments. As an example of the nonconventional information provided by Bohm's approach we can mention the controversial field of tunnelling times [29, 30]. References [22, 27] summarize several important aspects of the tunnelling times associated with Bohm trajectories.

4. A quantum Monte Carlo simulator: preliminary results

4.1. General considerations

As previously indicated, in order to consider large integration boxes without unnecessary computational burden, we have distinguished three regions in the device: the emitter region, the QW and the collector region (see figure 3). The emitter and collector regions, close to the corresponding contacts and characterized by smooth potential profiles, are treated as semiclassical regions. Here, the conventional MC technique is used to simulate the particle dynamics. The scattering mechanisms considered in these regions are (i) acoustic phonon scattering treated in the elastic approximation, (ii) polar optical phonon scattering and (iii) ionized impurity scattering, whose scattering rates are calculated using the usual parameters for GaAs. For simplicity, only the lower valley with a constant effective mass has been taken into account. On the other hand, we define the QW as the device region where the potential changes abruptly over distances shorter than the de Broglie wavelength. In this particular device, the QW includes the double-barrier region and its surroundings. The simulation of the electron transport in the QW is accomplished via Bohm trajectories associated with initial Gaussian wavepackets with different central wavevectors, k_c. In this particular simulation, 100 different initial Gaussian wavepackets (i.e. 100 different values of k_c) and 400 different stationary eigenstates are considered. At each time step of the MC procedure, ΔT, a table of 100×400 complex values has to be refreshed (which is the most significant additional effort needed to incorporate Bohm trajectories in our quantum MC simulator).

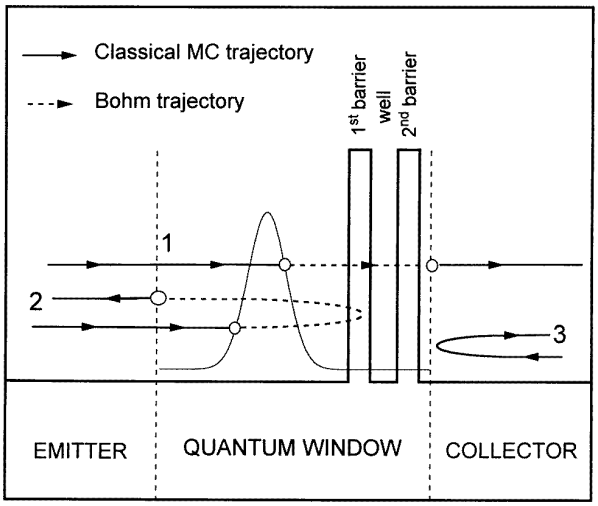

Figure 3. Schematic diagram of the simulated RTD showing the location of the QW and the double-barrier structure. Three different electron trajectories have been depicted to illustrate the classical-to-quantum matching model.

The selection of the main wavepacket parameters (x_c, k_c and σ_x as defined in equation (1)) requires the determination of a matching procedure. The whole wavepacket is included within the QW (i.e. the probability presence outside the QW is negligibly small) and the position x_c is chosen to be far enough from the first barrier (into the emitter) so that the potential profile is practically flat and the projection onto the basis of scattering eigenstates can be done analytically [31]. The selection of σ_x also requires a physical criterion since, as has been discussed, its value is related to the electron 'size'. (A practical and reasonable possibility is the choice of wavepackets wide enough in position ($\sigma_x \geqslant 25$ nm) so that the corresponding transmission coefficient is approximately that of the eigenstate associated with the central momentum, k_c. Equivalently, we could say that the wavepacket must be narrow in k-space as compared with the features of the local density of states [21].) Finally, the selection of k_c is based on the conservation of the particle's total energy [20]. A criterion based on momentum conservation has been discarded because the quantum potential introduces differences in the definition of the kinetic energy inside the QW with respect to the semiclassical approach [32]. Finally, let us note the intrinsic difficulties associated with the definition of such a matching criterion: we are actually trying to make a classical and a quantum picture for electrons simultaneously compatible.

In figure 3 we have represented three different trajectories to explain how the position continuity is also guaranteed. The circles represent the positions where the classical to quantum trajectory conversion takes place. The trajectory labelled by number 1 corresponds to one which is incident from the emitter and is finally transmitted. After choosing the initial position, the electron travels classically inside the QW (without scattering) until it arrives at x_0. Then, it follows the corresponding Bohm trajectory $x(x_0, t)$ until it exits the QW through the collector boundary. Similarly, trajectory number 2 corresponds to a particle incident from the emitter side which is finally reflected. We have also

depicted a trajectory incident from the collector (labelled by number 3) that it is classically reflected at the collector boundary of the QW because, in order to save computational time, we have only considered tunnelling from emitter to collector in this first version of the simulator.

At the present stage of the simulator, the effects of scattering in the device are only considered in the emitter and collector regions. This is clearly the main limitation of our simulator in its present implementation. Although in this paper we do not present our final choice for the introduction of scattering in the QW, some discussion is certainly required. Let us first discuss the evolution of an initial Gaussian wavepacket (equation (1)) in a flat potential. In particular, the group velocity can be found as $V_g = \hbar k_c/m^*$ (a parabolic dispersion relation is assumed) [23]. This result enables one to retrieve the classical description of the free particle, if the momentum and spatial dispersions are negligible (in other words, the centre of mass of the wavepacket moves like a particle which obeys the laws of classical mechanics). On the other hand, it is already well known that, while the momentum dispersion is a constant of motion, the spatial dispersion of the wavepacket varies with time and, for sufficiently long times, increases without limit (spreading of a wavepacket). This phenomenon is not limited to the special initial Gaussian wavepacket studied here but applies to any arbitrary free wavepacket. The spreading of the wavepacket is not taken into consideration in classical MC since it is implicitly assumed that collisions relocalize the particle. This result indicates that, apart from other physical reasons, the inclusion of scattering inside the QW is an unavoidable task in order to correctly simulate mesoscopic devices within our proposal. Nevertheless, as we will see in section 5, reasonable results can be obtained, even without scattering, if the QW length is small enough for the wavepacket spreading to remain within tolerable limits. Two quite different possibilities can be suggested for the introduction of scattering mechanisms inside the QW: (i) the definition of position-dependent scattering rates to model microscopic scattering between Bohm trajectories as a local event and (ii) the inclusion of scattering in the time evolution of the density matrix of single wavepackets. Although the actual evaluation of these possibilities is still being investigated, let us now discuss some general ideas.

In classical MC simulators, the scattering events are local (i.e. the position of the particle is continuous), but the scattering rates are calculated according to the Fermi golden rule (i.e. considering the matrix elements between completely extended plane waves). Having proposed an extension of the simulation based on real classical-like trajectories, it seems reasonable to look for a scattering model based on local transitions between trajectories. In this regard, two main aspects have to be considered: (i) position-dependent transition rates following the idea of Zimmerman and Yen [33] and (ii) a criterion for selecting the wavepacket (and the Bohm trajectory) after the collision event. However, although this proposal is intuitively clear, it hits the fundamentals of 'orthodox' Copenhagen interpretation of QM. So, more conventional proposals can also be considered. Among them, we mention the recent proposal of Rossi *et al* [18] which includes the scattering mechanisms in the evolution of the density matrix associated with single wavepackets. The development done in section 2, describing our model in terms of the density matrix, perfectly fits with this proposal.

4.2. Charge, phase-space distribution and current density

Provided that Bohm trajectories are calculated as explained in the previous sections (i.e. correctly selecting x_0 and taking the quantum potential into account), they can be treated as classical trajectories for all purposes. Therefore, the same method can be used to compute the charge and current densities in the QW and in the classical regions of the device. At every time step, of duration ΔT, the contribution of the ith particle to the charge density of the nth cell of width Δx_n ($x_n < x < x_n + \Delta x_n$) is computed by evaluating the fraction of the time step spent by the particle in this cell, $t_i(\Delta x_n)/\Delta T$. In particular, the charge contribution of the ith particle can be equal to unity if the particle remains inside the considered cell during the whole time step, or zero if the particle has not been present at all. An overall sum over the total number of particles N gives the electronic charge density associated with the specific cell at each time step:

$$\rho_n = \frac{\sigma}{\Delta x_n} \sum_{i=1}^{N} \frac{t_i(\Delta x_n)}{\Delta T} \tag{25}$$

where σ is the charge per unit area represented by each simulated particle. The obtained profile of the electronic charge density is used to update the potential at each time step by solving the Poisson equation (alternative methods for the assignment of the charge to the device mesh can be found in [34]) . An identical procedure can be used to obtain the momentum distribution of the particles at each cell by using an additional momentum grid at each spatial cell. Since the exact position and momentum of each particle (even in the QW) can be perfectly defined, we can compute the time spent by the ith particle in the phase-space cell ($x_n < x < x_n + \Delta x_n$ and $k_m < k < k_m + \Delta k_m$) during the simulated time T, $t_i(\Delta x_n, \Delta k_m)$. In this way, a time-averaged phase-space distribution $P(n, m)$ can be computed as

$$P(n, m) = \frac{1}{T\,\Delta x_n\,\Delta k_m} \sum_{i=1}^{N} t_i(\Delta x_n, \Delta k_m). \tag{26}$$

On the other hand, for a constant applied voltage, the instantaneous current density $J(t)$ can be computed as the sum of the instantaneous velocities $v_i(t)$ of all the $N(t)$ particles contained in the device:

$$J(t) = \frac{\sigma}{L} \sum_{i=1}^{N(t)} v_i(t) \tag{27}$$

where L is the total simulated length of the device [35]. By time averaging $J(t)$ one obtains the stationary current for a given applied voltage. The current density can also be computed as the time derivative of the net charge collected at the collector or emitter contacts, although in this way noisier results are obtained. The Ohmic model that we use for the emitter and collector contacts in our simulation is described

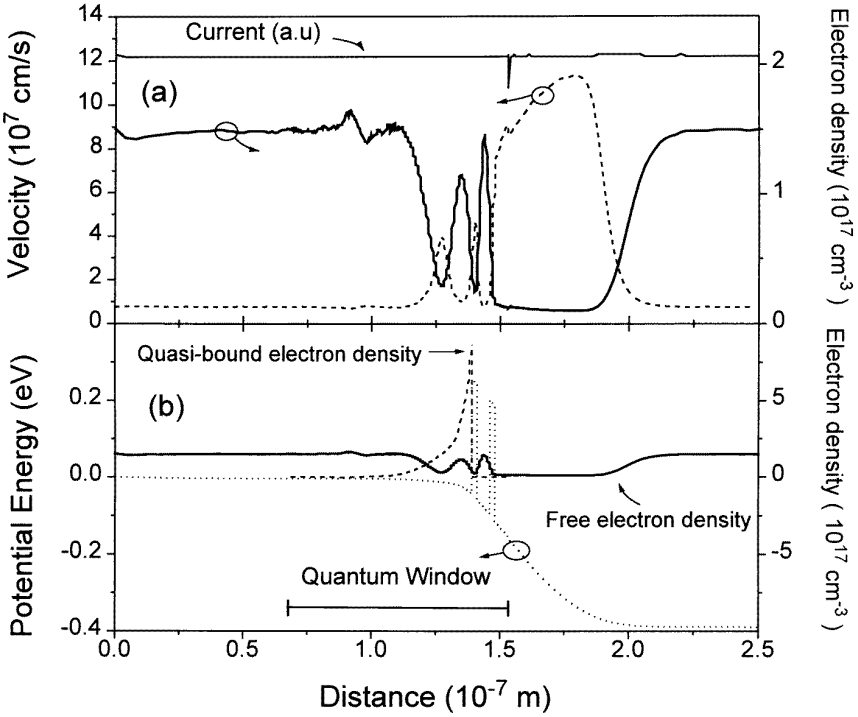

Figure 4. Self-consistent results of 3.0 nm/5.1 nm/3.0 nm double barrier GaAs/AlGaAs RTD at 77 K with an impurity density of 5×10^{18} cm^{-3} at a resonant bias of 0.39 eV. (*a*) Electron density (full curve) and average velocity (broken curve). The upper horizontal full curve represents the current density (in arbitrary units) computed as the product of the average charge density per average velocity. (*b*) Self-consistent potential profile (dotted curve) and electron density due to free electrons (full curve) and to quasi-bound electrons (broken curve).

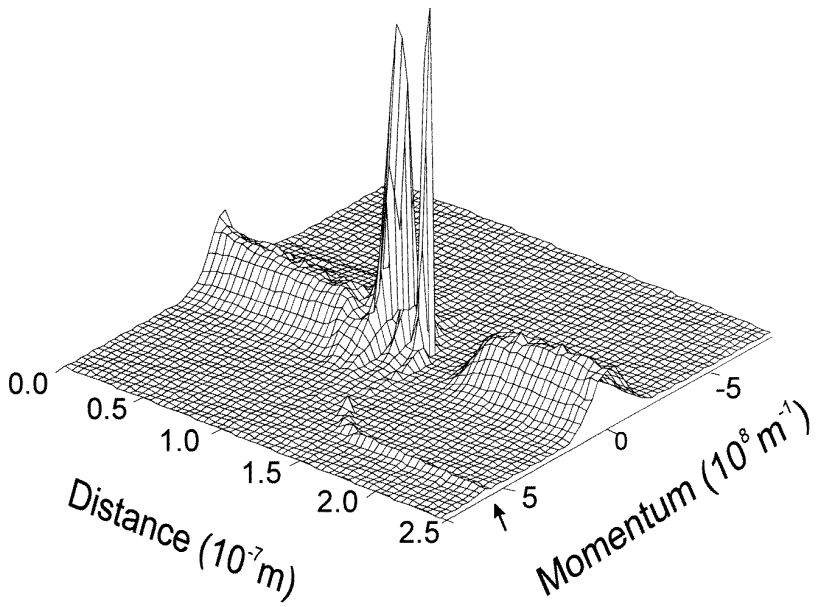

Figure 5. Phase-space distribution function along the whole device described in figure 4, just at the I–V peak current. Note the tunnelling ridge (indicated by an arrow), which originates in the QW as a result of resonant Bohm trajectories that are progressively thermalized in the collector by the scattering mechanisms.

in detail in [36]. Basically, if the cell adjacent to the contact is positively charged, carriers are injected from a velocity-weighted semi-Maxwellian distribution at equilibrium until the cell is charge neutral. On the other hand, if the cell is neutral or negatively charged, then the number of particles in the cell is left unchanged. Finally, let us emphasize that although the charge and current densities are calculated from individual trajectories, these reproduce the standard QM results. In other words, the self-consistent I–V characteristic would be the same if we had calculated it directly from time-dependent wavepackets, i.e. without using Bohm trajectories. These trajectories are just an adequate tool that perfectly

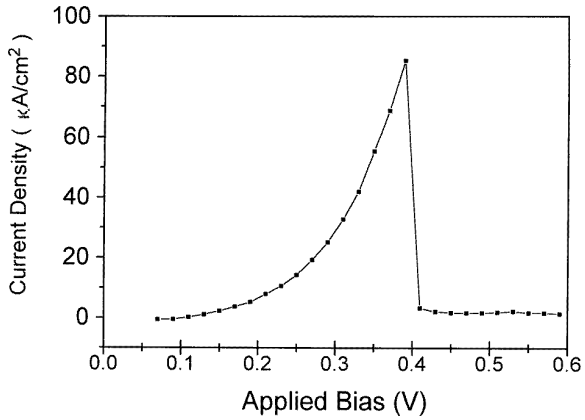

Figure 6. I–V curve of the double-barrier GaAs/AlGaAs RTD described in figure 4.

reproduces the dynamics of the wavepackets, providing a natural way to extend the classical MC technique to the QW.

5. Results

In this section we discuss the results obtained with our quantum MC simulator in order to demonstrate the feasibility of our proposal. The steady-state I–V characteristic of a typical GaAs/AlGaAs double-barrier structure with 3 nm barriers of 0.3 eV and a 5.1 nm well has been simulated at 77 K. For simplicity, only one valley with an isotropic effective mass of $0.067m_0$ has been taken into account to model the conduction band. The ionized impurity density in the GaAs electrodes is 1.51×10^{17} cm^{-3}, which corresponds to a realistic doping of $N_D = 5 \times 10^{18}$ cm^{-3} at 77 K. The AlGaAs barriers and the GaAs well have been considered to be undoped. The total simulation length is 0.25 μm divided into 366 cells. The classical emitter (68.5 nm) and collector (96.5 nm) regions are divided into a nonuniform mesh. On the other hand, the QW (84.9 nm) is divided into 283 cells of 0.3 nm each. Let us emphasize that the integration box is much larger than those typically used for solving the Liouville equation, since most of the device is simulated with a classical MC technique ([37] provides a larger box within the Liouville equation). As shown in figure 3, the QW extends asymmetrically at both sides of the double barrier because the emitter region of the QW has to be large enough to define the initial Gaussian wavepacket in a flat potential region.

Hereafter, in figures 4, 5 and 6, we show several results obtained for the double-barrier structure and the simulation parameters described above. First of all, we show self-consistent results obtained at a particular bias point of 0.39 V, corresponding to a position close to the peak of the I–V curve. The results shown in figures 4 and 5 were obtained by averaging instantaneous results over 1000 iterations after reaching the steady-state particle distribution (2000 iterations are usually required to reach it, the time step between iterations being $\Delta T = 5$ fs). In figure 4(a) we represent (full curve) the electron density, which exhibits pre-barrier oscillations and an accumulation in the well. No technical spurious discontinuities are detected at the boundaries of the QW, this being an indication of the smoothness of our classical-to-quantum matching model. By the broken curve we represent the average velocity, which is inversely proportional to the charge density, since their product must be position independent to ensure current uniformity along the device. In this regard, the behaviour in the collector depletion region is illustrative. It can be observed that the electrons travel faster in the depletion region because of the high electric field and, as a consequence, the electron density decreases in adequate proportion to maintain a uniform current. As reported by other authors [38], a depletion is also obtained in the emitter pre-barrier region as a consequence of the fact that electrons travel ballistically inside the QW. In this regard, the fact that no scattering is considered inside the QW has important consequences for the self-consistent results. To obtain an accumulation layer in the emitter region adjacent to the first barrier, the charge associated with quasi-bound states should be taken into account. However, since scattering in the QW is not considered yet, these states are unreachable from Bohm trajectories. To avoid this unphysical result, a semiclassical Thomas–Fermi approximation [39] has been used to compute this additional charge (see figure 4(b)). This electron charge is added to the MC charge obtained from expression (22) before solving the Poisson equation.

As we have previously discussed, in addition to results such as those obtained for charge and current densities, the use of causal trajectories allows one to obtain more information related to the hidden variables. In particular, the use of Bohm trajectories directly leads to the existence of a classical-like phase-space distribution (just as in the classical MC simulations). In figure 5 we have represented the particle phase-space distribution at the resonance voltage, obtained from expression (23) averaging over the last 1000 iterations. This distribution is qualitatively quite similar to the Wigner distribution function (WDF) solution of the Liouville equation [7–9, 36, 38], but it must be stressed that, contrarily to the WDF, our phase-space distribution is positive by construction. On the other hand, we notice the presence of a tunnelling ridge in the collector which was also reported within the WDF framework [38]. Electrons in the collector depletion region mainly come from Bohm trajectories associated with resonant wavepackets. Since these resonant trajectories behave ballistically, a number of electrons with large momentum appear in the collector. The presence of these resonant hot electrons, which are thermalized along the collector, is responsible for the net current density at the right boundary of the QW. On the contrary, the whole wavevector distribution is shifted towards positive momenta in the emitter, so as to give an uniform current density.

Finally, in figure 6 we present the self-consistently simulated current–voltage characteristic of the RTD described above. At the initial bias of 0.07 V, an arbitrary particle distribution is defined, and it evolves during 3000 iterations until the steady state is reached (lower voltages are not considered since no electron transport from collector to emitter is implemented). In order to reduce the transient time required to reach the steady state, the particle distribution obtained for one bias point is used as the seed for the next one. The current density is determined by averaging expression

(24) over the last 100 iterations. A sharp resonant peak is obtained in the I–V curve at an applied bias of 0.39 V. The whole I–V curve is very similar to that obtained from a fully coherent treatment based on the solution of the stationary effective-mass Schrödinger equation. This is an expected result since we are not considering scattering in the QW yet.

6. Conclusions

An extension of the MC device simulation technique has been presented to simultaneously deal with phase-coherence effects and inelastic scattering interactions in QM devices. Our proposal is based on the description of the QM dynamics via Bohm trajectories associated with time-dependent wavepackets.

The description of the constant flux of wavepackets, evolving coherently in the QW, is developed in terms of the density matrix. It is shown that, under steady-state situations and without considering scattering mechanisms, the nondiagonal terms of the density matrix remain zero in the basis of Hamiltonian eigenstates. This new formalism provides a new view for our proposal and allows us to compare it with previous models. Moreover, this new point of view suggests one way to implement the scattering mechanisms based on recent work [18].

The basics of Bohm's interpretation of QM have been reviewed, and the application of Bohm trajectories for the description of the tunnelling effect has been considered. It has been shown that stationary scattering eigenstates are not adequate for the description of the tunnelling dynamics and this has led us to the use of time-dependent wavepackets. Although Bohm's interpretation is a nonconventional QM theory based on a hidden causal structure, the results for charge and current densities are exactly the same that would be directly obtained by applying the methods of standard QM to the wavepackets. Since the final scope of a device simulator is the calculation of self-consistent current–voltage relationships at the external contacts, we can conclude that Bohm trajectories are an adequate tool for device simulation.

To illustrate the principles of our proposal, a self-consistent one-dimensional quantum MC simulator has been developed for RTDs. The proposed method restricts the QM treatment of electron transport to those regions of the device where the potential significantly changes in distances of the order of the de Broglie wavelength of the carriers (i.e. the QW). This has allowed us to consider large integration boxes (which reach the asymptotic contact regions where the potential profile is flat) without excessive computational burden. Inside the QW, Bohm trajectories associated with Gaussian wavepackets have been considered. Outside this region, the standard semiclassical MC technique has been implemented and, consequently, the electrons follow classical trajectories which allows a smooth matching of the individual classical and quantum trajectories. The use of a general and consistent QM description of transport is a substantial improvement over previous quantum MC approaches which considered *ad hoc* models [16].

In conclusion, we have demonstrated the feasibility of using time-dependent wavepackets and Bohm trajectories for the extension of MC simulators to deal with quantum devices. This kind of generalization of the semiclassical MC technique has the additional advantage of reaching the nanoelectronic range without abandoning the intuitive picture of carrier trajectories for the simulation of electron devices. Work is in progress towards the development of a complete quantum MC simulator for RTDs.

Acknowledgment

The authors are grateful to the Dirección General de Enseñanza Superior e Investigación Científica for supporting this work under the project numbers PB97-0182 and PB97-1331.

References

[1] Lüth H 1995 *Phys. Status Solidi* b **192** 287
[2] Reddy M, Martin S C, Molnar A C, Muller R E, Smith R P, Siegel P H, Mondry M J, Rodwell M J W and Allen S J Jr 1997 *IEEE Electron Device Lett.* **18** 218
[3] Mazumder P, Kulkarni S, Bhattacharya M, Sun J P and Haddad G I 1998 *Proc. IEEE* **86** 664
[4] Lake R, Klimeck G, Bowen R C and Jovanovic D 1997 *J. Appl. Phys.* **81** 7845
[5] Bowen R C, Klimeck G, Lake R K, Frensley W R and Moise T 1997 *J. Appl. Phys.* **81** 3207
[6] Pötz W 1989 *J. Appl. Phys.* **66** 2458
[7] Frensley W R 1990 *Rev. Mod. Phys.* **62** 745
[8] Kluksdahl N C, Kriman A M, Ferry D K and Ringhofer C 1989 *Phys. Rev.* B **39** 7720
[9] Jensen K L and Buot F A 1989 *J. Appl. Phys.* **65** 5248
[10] Biegel B A and Plummer J D 1997 *IEEE Trans. Electron Devices* **44** 733
[11] García-García J, Oriols X, Martin F and Suñé J 1996 *Solid State Electron* **39** 1795
[12] García-García J, Oriols X, Martin F and Suñé J 1998 *J. Appl. Phys.* **83** 8057
[13] Jauho A P and Wilkins J W 1984 *Phys. Rev.* B **29** 1919
[14] Datta S 1990 *J. Phys.: Condens. Matter* **2** 8023
[15] Gullapalli K K, Miller D R and Neikirk D P 1991 *Tech. Dig. IEDM* 511
[16] Salvino R E and Buot F A 1992 *J. Appl. Phys.* **72** 5975
[17] Fischetti M V 1998 *J. Appl. Phys.* **83** 270
[18] Rossi F, Di Carlo A and Lugli P 1998 *Phys. Rev. Lett.* **80** 3348
[19] Burgnies L, Vanbésien O, Sadune V, Lippens D, Nagle J and Vinter B 1994 *J. Appl. Phys.* **75** 4527
[20] Oriols X, García J J, Martin F, Suñé J, González T, Mateos J and Pardo D 1998 *Appl. Phys. Lett.* **72** 806
[21] Ashcroft N W and Mermin N D 1976 *Solid State Physics* (NY: Holt, Reinhart and Winston)
[22] Oriols X, Martín F and Suñé J 1996 *Solid State Commun.* **99** 123
[23] Cohen-Tanoudji C, Diu B and Laloë F 1977 *Quantum Mechanics* (New York: Wiley)
[24] See equation (6.26) in Leavens C R and Aers C G 1993 Bohm trajectories and the tunneling time problems *Scanning Tunneling Microscopy III* ed R Wiesendanger and H-J Güntherodt (Berlin: Springer)
[25] Bohm D 1952 *Phys. Rev.* **85** 166
[26] Holland P R 1993 *The Quantum Theory of Motion* (Cambridge: Cambridge University Press)
[27] Leavens C R and Aers G C 1993 *Scanning Tunneling Microscopy III* ed R Wiesendanger and H-J Güntherodt (New York: Springer) pp 105–40

[28] Oriols X, Martín F and Suñé J 1996 *Phys. Rev.* A **54** 2594
[29] Hauge E H and Stovneng J A 1989 *Rev. Mod. Phys.* **61** 917
[30] Landauer R and Martin T 1994 *Rev. Mod. Phys.* **66** 217
[31] Dumont R S and Marchioro T L II 1993 *Phys. Rev.* A **47** 85
[32] Baker J R 1994 *Semicond. Sci. Technol.* **9** 991
[33] Zimmermann and Yen W 1987 *Rev. Phys. Appl.* **22** 99
[34] Jacoboni C and Lugli P 1989 *The Monte Carlo Method for Semiconductor Device Simulation* (New York: Springer)
[35] Gruzinskis V, Kersulis S and Reklaitis A 1991 *Semicond. Sci. Technol.* **6** 602
[36] González T and Pardo D 1996 *Solid State Electron.* **39** 555
[37] García-García J, Martín F, Oriols X and Suñé J 1998 *Appl. Phys. Lett.* at press
[38] Frensley W 1989 *Solid State Electron.* **32** 1235
[39] López-Villanueva J A, Melchor I, Gámiz F, Banqueri J and Jiménez Tejada J A 1995 *Solid State Electron.* **38** 203